Applied Thermal Engineering 213 (2022) 118693

Contents lists available at ScienceDirect

Applied Thermal Engineering

journal homepage: www.elsevier.com/locate/apthermeng

Experimental tests on the performance of an economic model predictive control system in a lightweight building

Jacopo Vivian [a,c,*], Lorenzo Croci [b], Angelo Zarrella [a]

[a] University of Padua, Dept. of Industrial Engineering - via Venezia 1, 35131 Padua, Italy
[b] Ricerca Sistema Energetico SpA, Dept. of Power System Development - via Rubattino 54, 20134 Milan, Italy
[c] EMPA Materials Science and Technology, Urban Energy Systems Lab - Ueberlandstrasse 129, 8600 Dübendorf, Switzerland

ARTICLE INFO

Keywords:
Model Predictive Control
All-electric buildings
Air-source heat pumps
PV self-consumption
Energy flexibility

ABSTRACT

European policies are fostering the electrification of energy use, including space heating and cooling systems, in order to decarbonise the building stock. The significant penetration of electrical loads and domestic photovoltaic (PV) plants has therefore become an important topic for researchers and engineers working in the building sector. In this context, this paper presents a recently constructed laboratory for testing efficient management strategies in all-electric houses. The article describes the laboratory and the Model Predictive Control (MPC) strategy developed to minimize economic costs for space heating while ensuring thermal comfort in the indoor environment with a simulated rooftop PV system. The proposed controller leverages prior knowledge about the physical and geometric properties of the building and the optimization problem is formulated using mixed-integer quadratic programming. This article reports the results of calibration and optimization performed in open loop, as well as two closed loop tests where the MPC controls the HVAC system using receding horizon. The predictive controller was able to substantially increase PV self-consumption in both tests compared to a conventional thermostat, thus cutting electricity costs for heat pump by 10–17%. Such improvement was obtained at the price of a higher thermal comfort violations, mainly due to oversimplified HVAC system models. In light of these findings, the article analyses the effect of such simplifications and suggests possible alternative modelling approaches.

1. Introduction

It is widely accepted that the large-scale deployment of heat pumps is a promising way toward the decarbonisation of the heating sector. This trend will severely affect the power consumption patterns in the electrical distribution systems [1]. At the same time, increasing penetration of small-scale renewable energy sources such as domestic PV systems is pushing the energy system towards a decentralised structure [2]. In this context, Building Energy Management Systems (BEMS) play a key role as they can shift energy consumption towards the most convenient time windows using the available energy flexibility sources, such as batteries, thermal storage tanks, heat emission systems and building structures [3]. The latter can be used both in the heating and in the cooling season and their effectiveness depends on the trade-off between efficiency, thermal comfort and the service they are meant to provide [4]. BEMS may pursue individual objectives, such as cutting costs or increasing autarky of single buildings [5] or system-level objectives, such as reducing peak loads on electrical distribution grids [6] or providing ancillary services to the power grid [7]. Several techniques can be used to control technical systems in buildings. Currently, most commercial products rely on Rule-Based Controllers (RBC) that react on disturbances using simple heuristics to maintain HVAC systems within pre-defined boundaries. The latter are usually set to achieve safe and efficient operation based on manufacturers and installers' experience, and to provide acceptable levels of indoor environmental quality. Model Predictive Control (MPC) is a well-established method for constrained control and recently has been receiving extensive attention from researchers in the field of control of buildings [8]. MPC takes advantage from the prediction of future disturbances (weather, internal heat gains etc.) given some feasible ranges for the controlled variables. The underlying optimization is able to overcome RBC controllers and fully exploit the energy flexibility of building structures and thermal storage systems using heat pumps [9]. Despite its potential, MPC has not yet gained a significant share of the building controls market, mainly due to the significant engineering effort needed to implement and configure a

* Corresponding author at: University of Padua, Dept. of Industrial Engineering - via Venezia 1, 35131 Padua, Italy.
E-mail addresses: jacopo.vivian@empa.ch, jacopo.vivian@unipd.it (J. Vivian).

https://doi.org/10.1016/j.applthermaleng.2022.118693
Received 19 December 2021; Received in revised form 20 March 2022; Accepted 17 May 2022
Available online 21 May 2022

Nomenclature

Symbols

α	Absorptance [-]
H	Heat exchange coefficient [W/K]
c	Operating cost [€/kWh]
C	Thermal capacitance [J/K]
Φ	Heat flow rate (actual) [W]
Q	Heat flow rate (calculated) [W]
I	Irradiance [W/m^2]
θ	Temperature [°C]
n	Speed [Hz]
w	Power [W]
δ	Temperature difference [°C]
λ	Price [€/kWh]
γ	Weight (coefficient in the obj. function)
V	Volume [m^3]
τ	Sampling time [s]
k	Constant coefficient (generic)
N	Integer number (time steps or days) [-]
TD	Thermal discomfort index [°C/day]
u	On-off signal (0–1)

Subscripts/superscripts

buy	buy (purchase)
c	calibration
conv	convective
d	daily
i	Indoor air
int	Internal heat gain
e	External air
e,eq	Sol-air
el	electrical
H	Horizon
hc	Heating/cooling load
pred	Predicted (from forecast)
hp	Heat pump
hs	Heat storage
m	Thermal mass
max	maximum
meas	measured
min	minimum
mpc	Model Predictive Control
od	other devices
opt	optimal
out	output
pv	photovoltaic
s	Internal surfaces
se	External surfaces
self	Self-consumption
sell	Sell (sale)
sol	Solar
su	Start-up
sup	Supply air
t	Time
tr	Transmission
ts	Thermostat control
u	Input penalty
ve	Ventilation

Abbreviations

BEMS	Building Energy Management System
COP	Coefficient of Performance
DHW	Domestic Hot Water
HVAC	Heating, Ventilation, Air Conditioning
MPC	Model Predictive Control
PID	Proportional Integral Derivative
PV	Photovoltaic
RBC	Rule Based Control
RMSE	Root Mean Square Error

controller model that can be adapted to different buildings and HVAC systems. Serale et al. [10] classified research on MPC in buildings according to the objective function adopted, and found out that most of the proposed formulations include operational costs and thermal comfort terms. When costs are included in the objective function, the optimal control problem can be referred to as Economic MPC (EMPC).

Zong et al. [11] presented a discussion on the challenges for economic MPC such as forecast availability, practical constraints due to implementation on hardware etc. They have tested the proposed EMPC in a building lab with radiators and compared it to a simulated PID controller under the same boundary conditions, though the quantitative result of such comparison is not quantitatively assessed. Blum et al. [12] investigated the impact of seven factors (building design, model structure, model order, data set, data quality, identification algorithm and initial guesses) on the model accuracy and on the performance of an MPC for cooling purposes. They discovered that a difference of up to 20% in cooling cost can occur between the best performing model and the worst one. The primary factors contributing to this result were model structure and initial parameter guesses during parameter estimation of the model.

1.1. Simulation-based research on MPC performance

Verhelst et al. [13] showed that simplifications of the heat pump characteristics, i.e., neglecting the dependency of the heat pump efficiency on the compressor frequency and the supply water temperature, is only permitted if the square of the predicted energy cost is penalized in the cost function. This way, high fluctuations of the heat pump thermal power, which negatively affect the control performance, are avoided. They also found the cost function to be very flat near the optimal solution, since different optimal control formulations yielded slightly different control profiles while resulting in similar energy cost and thermal discomfort. Hu et al. [14] developed MATLAB-TRNSYS co-simulation tests to compare an MPC controller to a conventional on–off control for a building with floor heating system. They found out that MPC is able to implement automatic and optimal preheating, thus improving thermal comfort at the beginning of occupancy, reducing the energy consumption during peak periods, and to reduce the daily electricity costs by 2–19% for residential end-users. Bianchini et al. [15] simulated the participation of two buildings of different size in a Demand Response program using MPC with receding horizon and EnergyPlus models for simulating real-world feedback signals. They demonstrated that it is possible to obtain suboptimal results by means of heuristic strategies with negligible loss of accuracy. In a later work, they demonstrated that forecast uncertainty can increase costs by up to 8% compared to solutions with exact forecasts, which is approximately one third of the cost savings obtained for their case study compared to a thermostat controller [16]. According to the authors, this is a consequence of the receding horizon strategy, which implies that only the prediction errors occurring in the near future significantly affect the performance. Drgona et al [17] used neural networks to mimic the behavior of MPC to control thermal comfort and energy consumption in a case-study building with six thermal zones. Approximating MPC led to suboptimal decisions able to overcome the performance of rule-based

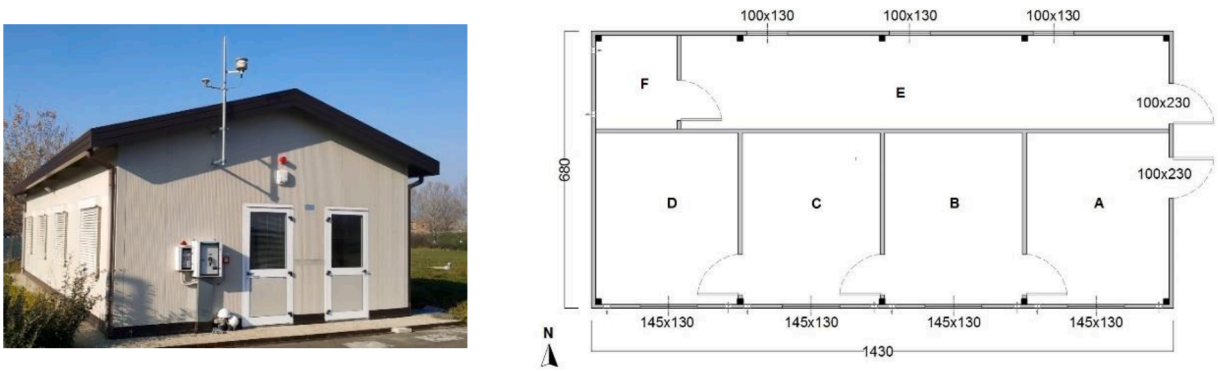

Fig. 1. (a) Photo and (b) floor plan of the lab.

controllers. Kuboth et al [18] developed a distributed MPC problem to minimize costs for a simulated single-family house. The MPC was able to reduce costs by 11.6% compared to a PID controller through an increase of COP, a reduction of auxiliary heater operation, an increase in photovoltaic self-consumption. Wang et al [19] proposed a nonlinear optimization to coordinate the operation of fans, pumps and chiller in a building equipped with a chiller-based AHU system. Simulations demonstrated that the proposed MPC achieved 6.2% energy consumption savings and 12.3% electricity bill reduction compared to a traditional PI control. Kishore et al [20] studied different precooling strategies to manage the heat gains in lightweight building walls integrated with phase-change materials. They showed that while without PCM the load shifting is limited, its integration in a lightweight building envelope results in a significant shift of the peak load at the price of higher heat gains. Therefore, a trade-off must be pursued to optimally manage cooling loads in these buildings. A similar study was proposed by Cesari et al [21], that evaluated the performance of PCMs integrated in a radiant floor system in a lightweight building. Simple heuristics based on weather forecasts were proposed to avoid overheating and reduce energy consumption. Simulations showed that 4–8% energy consumption could be saved, and that prediction horizons of 6 and 12 h were sufficient for the heating and cooling period, respectively. Mirakhorli and Dong [22] simulated electrical loads of 15,000 buildings with both MPC and traditional control. Each building was equipped with air conditioning, water heater, electric vehicles, PV and battery. The study showed that MPCs can be used for an aggregated price-based load control provided that a suitable nodal price is communicated to the buildings, and that penalties for voltage drops help maintain a stable operation of the distribution grid. MPC-based integration was capable of reducing the peak load by 17% and saved the generation cost by 21%, while buildings were able to save 22% in their operation cost. Golmohamadi et al [23] formulated a three-stage stochastic programming problem to schedule, adjust, and regulate responsive heat pumps hierarchically to allow their participation to day-ahead and intraday electricity markets as well as to balancing markets. A numerical example demonstrated that the proposed approach can provide flexibility to the system and at the same time reduce energy costs (up to 47%) in a Danish single-family house. Hou et al [24] formulated a nonlinear MPC and tested it via simulations using a University building in Norway as a case study. They demonstrated that incorporating a forecast error model in the MPC allows to achieve almost the same cost savings of an MPC with perfect forecasts, whereas the performance without error model led to a significantly reduced cost saving and an increase in thermal comfort violations compared to the RBC. Lee et al [25] proposed an MPC with increasing levels of detail for the variable-speed heat pump model. Simulations of the heat pump over the whole heating season showed that both energy consumption and energy supply costs are heavily affected by the complexity of the heat pump model. Similarly, Wang et al [26] proposed a nonlinear MPC control strategy for an ASHP using water temperature difference as one of the controllable inputs. They obtained a slight improvement of the energy saving over reference PI controllers when compared to simpler MPC formulations.

1.2. Experimental research on MPC performance

Joe and Karava [27] demonstrated that in an office with radiant floor a data-driven MPC could lead to 34% cost savings compared to baseline feedback control during the cooling season and 16% energy use reduction during the heating season. Fiorentini et al [8] proposed a two-level comfort-oriented control strategy where the higher level assessed the possibility to operate in natural ventilation mode and the lower level optimised the HVAC system operation. The control strategy was able to improve comfort and reduce energy consumption compared to benchmark controllers, as demonstrated both via experiments and simulations. Afram et al [28] proposed a supervisory MPC controller to find the optimum set-points trajectories based on the weather forecast and electricity prices for a typical house in Ontario (Canada) equipped with radiant floor heating, air handling units and a ground source heat pump. Simulations and experimental results showed that cost savings at least 16% could be obtained in the cooling season, and that during the heating season the cost savings caused by load shifting to off-peak hours was significant only during moderate weather, i.e. when the external temperature was higher than 5 °C. Bünning et al [29] used data-driven models within a convex optimization to control the room temperature in a living lab. Compared to a conventional hysteresis controller, the data-driven MPC approach saved 25% of cooling energy while reducing comfort constraint violations by 72% in a six-day experiment. Experiments with longer control horizons suggested that the applicability for commercial buildings might be limited. In another study, Bünning et al [30] demonstrated that robust MPC based on data-driven models can also be used to provide frequency regulation reserves using a heat pump and warm buffer tank. Fiorentini et al [31] proposed a Hybrid Model Predictive Control (HMPC) strategy to manage a PVT-assisted HVAC system in an Australian residential building equipped with a phase change material (PCM) active storage unit, integrated with a standard ducted air conditioning system. The experiments showed the HMPC was able to reduce the energy consumption especially in the cooling season due to enhanced natural ventilation and higher EER of the heat pump. Serale et al [32] formulated and implemented a similar model predictive control strategy for the optimal management of a latent heat thermal energy storage unit coupled with a solar thermal collector and a backup electric heater. The study relied on piecewise linearization to describe the solid–liquid phase change of the PCM slurry. The proposed MPC strategy allowed to achieve significant energy savings compared to rule-based controllers.

1.3. Research gap and objectives

Despite the considerable number of research papers on MPC applied to buildings, two research gaps emerged from the literature review. In

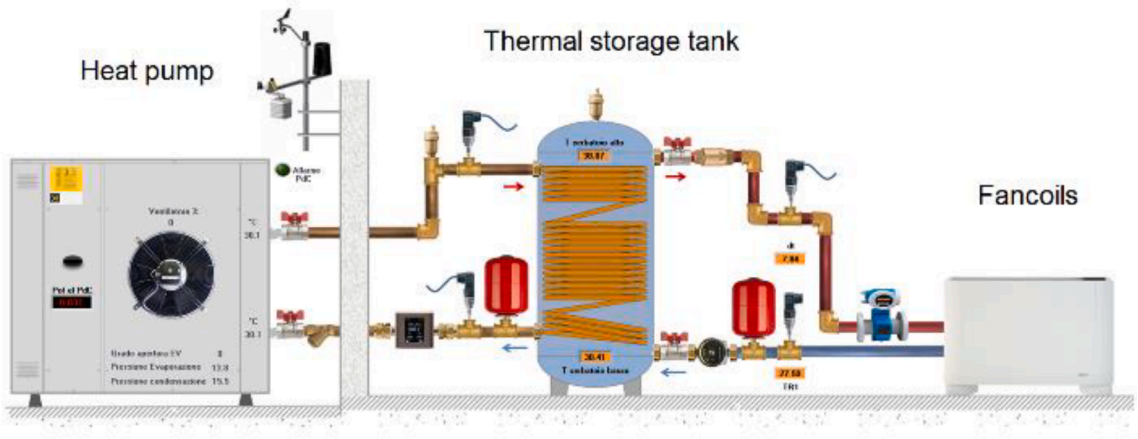

Fig. 2. Synoptic panel of the HVAC system.

fact, to the best of our knowledge, only two research papers so far have discussed the impact of heat pump/HVAC system models on the MPC performance [25,26], and none of them relied on experimental tests. Moreover, the majority of the reviewed papers applied this control approach to heavyweight building structures and heat emission systems with slow thermal response (e.g. radiators, floor heating systems). Therefore, this paper investigates HVAC systems modelling issues for MPC applied to a lightweight building with a fast-responsive heat emission system (fan coils). This paper aims at filling these research gaps in the ongoing discussion on economic MPC performance. It reports the results of the implementation of an economic MPC experimentally applied to a lightweight building lab located in Piacenza (Italy). The effects of the simplifications introduced by linearizing HVAC system models (heat pump, thermal storage and fan coils) are discussed using data obtained during operation.

2. Lab description

The experiments were carried out in the laboratory shown in Fig. 1, that was built to benchmark the performance of "all-electric" buildings. To this end, the laboratory has been equipped with (i) an air-to-water heat pump air conditioning system connected to four fan coils with a 300-liter water heat storage tank; (ii) a heat pump water heater with 200-liter storage tank for domestic hot water (DHW) production; (iii) an air/air conditioning system consisting of an outdoor condensing unit and four indoor units with a nominal cooling capacity of 6.8 kW; (iv) four air extractors; (v) a set of electrical appliances (e.g., washing machine, dryer, dishwasher and combined refrigerator). The perimeter walls and the roof are made up of polyurethane prefabricated panels. The external walls also have 2.5 cm plasterboard on the inner surface. Above the concrete slab, the ground floor has 5 cm insulation and 5 cm screed that also contribute to the building's thermal inertia. The net height of the rooms is 2.7 m, and they are separated from the attic by a false ceiling made by mineral fiber panels. Only rooms A, B, C and D have been considered in this work, since rooms E and F are used for different purposes and their heating and cooling system could not be controlled. The total conditioned area is therefore 59.4 m^2. Further information on the stratigraphy of the building components can be found in Appendix A.

The HVAC system is illustrated in Fig. 2. In the upcoming months, the laboratory will be also equipped with a PV system with inverter and storage battery. In the meanwhile, the PV system has been simulated –see PV model section. A monitoring system allows to read data logged by the environmental sensors such as temperatures, mass flow rates, heat and power flow and automatically controls the system and communication with the heat pump. The software was created in the LabView environment based on a personal computer and on Advantech

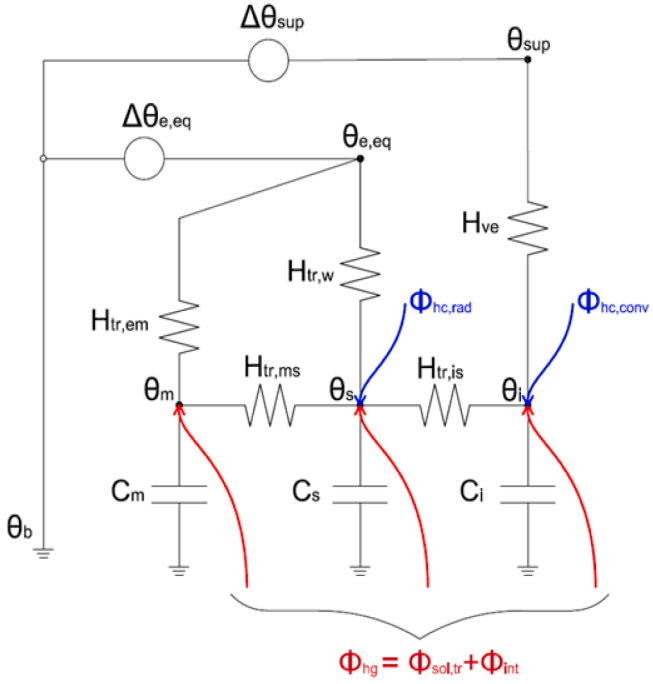

Fig. 3. 5R3C model of the building.

acquisition modules. The communication architecture uses Modbus ASCII and Modbus RTU fieldbuses on RS485 network. A preliminary analysis on the energy performance of the lab based on EnergyPlus simulations showed that the specific annual energy needs are approximately 68 kWh/m^2 for heating and 13 kWh/m^2 for cooling, including both sensible and latent loads. The whole analysis has not been included in this article to facilitate its readability.

3. Models

3.1. Building model

The lumped capacitance model used to reproduce the thermal behavior of the lab is a modified version of the well-known model proposed by Standard ISO 13790 [33]. The Standard uses the electrical analogy and distributes the heat gains to three temperature nodes of an equivalent thermal network: Φ^{ia} to the indoor air temperature node (θ^i), Φ^{st} to the surface temperature node (θ^s) and Φ^m to the thermal mass temperature (θ^m) node. The modified model has a thermal capacitance

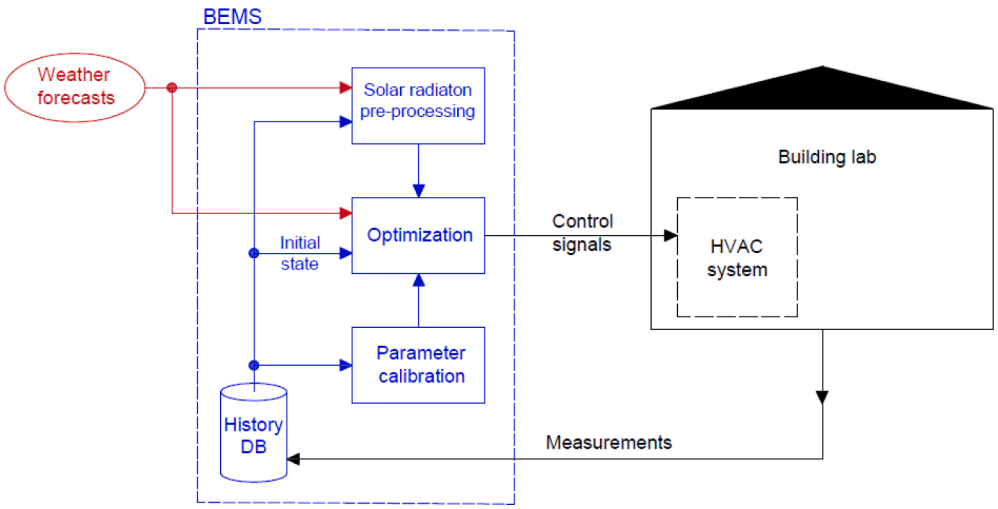

Fig. 4. Qualitative scheme illustrating the BEMS architecture.

in each temperature node, thus being a 5R3C model, as shown in Fig. 3. The heat loads derive from the sum of HVAC heat output Φ^{hc}, solar heat gains Φ^{sol} and internal heat gains Φ^{int}. The internal heat gains have been assumed equal to a constant heat flow rate $\Phi^{int,0}$. The indoor air temperature can then be found by solving the linear system given by the energy balance on the mentioned temperature nodes:

$$H_{ve}(\theta_t^{sup} - \theta_t^i) + H_{tr,is}(\theta_t^s - \theta_t^i) + \Phi_t^{ia} + f_{conv}\,\Phi_t^{hc} = \frac{C_i}{\tau}(\theta_t^i - \theta_{t-\tau}^i) \quad (1)$$

$$H_{tr,w}(\theta_t^{e,eq} - \theta_t^s) + H_{tr,is}(\theta_t^i - \theta_t^s) + H_{tr,ms}(\theta_t^m - \theta_t^s) + \Phi_t^{st} + (1 - f_{conv})\,\Phi_t^{hc} = \frac{C_s}{\tau}(\theta_t^s - \theta_{t-\tau}^s) \quad (2)$$

$$H_{tr,em}(\theta_t^{e,eq} - \theta_t^m) + H_{tr,ms}(\theta_t^s - \theta_t^m) + \Phi_t^m = \frac{C_m}{\tau}(\theta_t^m - \theta_{t-\tau}^m) \quad (3)$$

where the capacitance terms C_i, C_s and C_m represent the thermal inertia offered by the indoor air volume, by the lightweight components (furniture, internal partitions etc) and by the structural elements of the building (walls, floor, ceiling etc). The other building parameters are the ventilation heat transfer coefficient H_{ve}, the coupling conductance between internal air and surface node $H_{tr,is}$, the thermal transmission coefficients of the windows $H_{tr,w}$ and of the opaque building components $H_{tr,op}$. The latter is divided into two components, $H_{tr,em}$ and $H_{tr,ms}$. The air supply temperature due to infiltration and/or ventilation (θ^{sup}) is equal to the external air temperature (θ^e) since there is no mechanical ventilation system and f_{conv} is a parameter that accounts for different radiative and convective contributions of HVAC terminals (example: $f_{conv} = 1$ for fancoils, $f_{conv} = 0.5$ for radiators).

Another important difference between this model and the Standard is that here the solar heat gains consider only the radiation transmitted through the glazed surfaces $\phi_{sol,tr}$. Solar radiation absorbed by exterior opaque surfaces was considered through a sun-air equivalent temperature $\theta_{e,eq}$, which is a common assumption for simplified building energy models, calculated as follows:

$$\theta_t^{e,eq} = \theta_t^e + \frac{\alpha_{se}\, I_t^{sol,se}}{h_{conv,se}} \quad (4)$$

The model assumes that the four rooms of the lab can be modelled as a single thermal zone. This assumption is justified by two reasons: (i) the four fan coils cannot be controlled separately and (ii) all the windows are oriented towards the South. Since internal heat gains do not give a significant contribution due to the absence of people in the lab during the experiments, the indoor air temperature profile should not present significant differences in the four rooms. Monitored data have confirmed this hypothesis, with the highest local deviations of indoor temperature recorded in room A due to door openings.

3.2. Heat pump model

The simplified steady-state model adopted for the air source heat pump consists of three equations. The first equation correlates the heat pump capacity, i.e. the maximum thermal power output, to temperatures of the heat source (external air) and heat sink (thermal storage tank). In general, the polynomial law used for this correlation may be of the first, second or third order. Eq. (5) shows the polynomial of the second order. Eq. (6) assumes that the thermal power output is a fraction of the capacity equal to the ratio between the compressor speed n and the maximum speed n_{max}. Finally, Eq. (7) assumes that the power consumption of the heat pump including auxiliaries can be calculated based on a polynomial similar to Eq. (4), where COP is the coefficient of performance of the heat pump.

$$Q_t^{hp,max} = a_0 + a_1\theta_t^e + a_2\theta_t^{hs} + a_3\theta_t^{e2} + a_4\theta_t^{hs2} + a_5\theta_t^e\theta_t^{hs} \quad (5)$$

$$\Phi_t^{hp} = \frac{n}{n_{max}} Q_t^{hp,max} \quad (6)$$

$$COP_t = b_0 + b_1\theta_t^e + b_2\theta_t^{hs} + b_3\theta_t^{e2} + b_4\theta_t^{hs2} + b_5\theta_t^e\theta_t^{hs} \quad (7)$$

In order to avoid the introduction of nonlinear constraints, the values for θ_t^{hs} have been obtained by replacing the optimal values calculated for each time t at the last optimization run.

3.3. PV system model

While the previous models were included among the constraints of the optimization problem, the photovoltaic system model replaces the real system, i.e. provides power production values depending on the forecasted solar radiation. The model used was taken from an open-source collaborative project called pvlib [34], which is based on the well-known clear sky model [35]. The simulated PV system is assumed to be positioned on the south-oriented side of the roof, with a tilt angle of 20°. It consists of 14 modules with 220 W nominal power.

4. Methods

4.1. BEMS architecture

The Building Energy Management System (BEMS) was developed in Python with the logic of object oriented programming. It consists of

Table 1
Calibrated parameters in the grey-box building model.

#	Parameter	Unit	Description
1	C_m	[J/K]	Thermal capacitance of heavy building components (walls, floors, etc.)
2	$H_{tr,em}$	[W/K]	Heat exchange coefficient due to transmission through opaque walls on the external side
3	$H_{tr,is}$	[W/K]	Heat exchange coefficient due to transmission between indoor air and surfaces
4	$H_{tr,ms}$	[W/K]	Heat exchange coefficient due to transmission through opaque walls on the internal side
5	$H_{tr,w}$	[W/K]	Heat exchange coefficient due to transmission through windows
6	H_{ve}	[W/K]	Heat exchange coefficient due to ventilation and/or infiltration
7	f_{conv}	[-]	Convective heat exchange rate of HVAC system terminal units
8	$k_{s,gla}$	[-]	Multiplicative factor for the solar radiation transmitted through transparent surfaces
9	$k_{s,opa}$	[-]	Multiplicative factor for the solar radiation absorbed by opaque surfaces
10	$\Phi_{int,0}$	[W]	Average internal heat gain due to people, lights and appliances
11	$k_{fg,1}$	[-]	Distribution coefficient for internal and solar heat gains (n.1)
12	$k_{fg,2}$	[-]	Distribution coefficient for internal and solar heat gains (n.2)
13	C_s	[J/K]	Thermal capacitance of lightweight building components (partitions, furniture, etc.)
14	C_i	[J/K]	Thermal capacitance of heated/cooled air volume

several processes that are cyclically run on the computer of the lab where all measurements are collected. These processes include: (i) reading measurements from the plant and environmental sensors; (ii) reading weather forecast and update PV production forecasts accordingly; (iii) calibrating parameters of the lumped capacitance model; (iv) scheduling the HVAC system operation for next hours. As Fig. 4 shows, the BEMS relies on a model predictive control loop. Measurements of indoor and outdoor temperature, solar radiation and heat flow rate released from the HVAC plants to the indoor environment are stored in a history database. All these measurements are used to calibrate a lumped capacitance building model described in the Models Section. The calibration process carried out to find the parameters of the building model is described in the Methods section. Instead, the calibration of the heat pump model consists in the calculation of the coefficients of polynomials $a_1..a_N$ and $b_1..b_N$ through a linear regression –see Eq. (5–7). Once the optimal parameters are found through these calibration procedure, they are used to build the constraints of an optimization problem described hereafter. The optimization relies on weather forecasts that are updated by an external service twice a day.

4.2. Calibration of the building model

The calibrated parameters are those found in Equations (1)–(3). More specifically, the parameters are five thermal conductances, three thermal capacitances, and six other auxiliary parameters for a total of fourteen parameters, as shown in Table 1. The auxiliary parameters modify the effect of the boundary conditions on the thermal response of the building: the convective share of the thermal load yielded by the system to the environment f_{conv}, the shares of solar radiation transmitted through the glazed surfaces and absorbed by the opaque ones $k_{s,gla}$ and $k_{s,opa}$, the internal loads due to people, lights and electrical appliances $\Phi_{int,0}$ and two coefficients ($k_{fg,1}$ and $k_{fg,2}$) that determine the distribution of solar and internal loads on the temperature nodes as given in Eqs. (8)–(10).

$$\Phi_t^{ia} = 0.5\Phi_{int,0} + k_{fg,2}\Phi_t^{sol,tr} \tag{8}$$

$$\Phi_t^{st} = \left(1 - k_{fg,1}\right)\left[0.5\Phi_{int,0} + \left(1 - k_{fg,2}\right)\Phi_t^{sol,tr}\right] \tag{9}$$

$$\Phi_t^{m} = k_{fg,1}\left[0.5\Phi_{int,0} + \left(1 - k_{fg,2}\right)\Phi_t^{sol,tr}\right] \tag{10}$$

The calibration is the numerical process by which the parameters describing the building's dynamic thermal behaviour in Eqs. (1)–(3) are initially determined based on an approximate knowledge of the building physical and geometrical properties, and then iteratively recalculated to ensure that the lumped capacitance model described above adheres as much as possible to the real behaviour of the building. This operation is carried out by an optimisation algorithm that minimises the mean square error between the average indoor air temperature profile measured in the lab and the indoor air temperature calculated by the mentioned model. Thus, the objective function is:

$$\min_{x\in X}\sqrt{\frac{\sum_{t=1}^{N_c}\left(\theta_t^i(x) - \theta_t^{i,meas}\right)^2}{N_c}} \tag{11}$$

where x is the optimal set of parameters [C_m, $H_{tr,em}$, $H_{tr,is}$, $H_{tr,ms}$, $H_{tr,w}$, H_{ve}, f_{conv}, $k_{s,gla}$, $k_{s,opa}$, $\Phi_{int,0}$, k_a, k_s, C_s, C_i] and N_c is the length of the training (calibration) period. The calibration algorithm, i.e., the optimization method used to minimize the objective function above, is the Trust Region Reflective algorithm contained in the Python library scipy.optimize.least_squares [11]. This library is based on algorithms suited to solve problems in which the objective function takes the nonlinear convex form:

$$\min_{x\in X}\sum_{t=1}^{N_c} f(x^2) \tag{12}$$

in which the decision variables are constrained in a finite domain defined $x \in [l_b, u_b]$. Two exit criteria from the iterative loop were set: when in two consecutive iterations the difference between the objective function is 0.0005%, or when the maximum number of iterations (set to 500) is reached.

4.3. Optimization problem

The current version of the BEMS controls only the heat pump and the circulation pump of the secondary water loop (see Fig. 2). In the future, also the DHW boiler and other electrical devices will be integrated within the BEMS. The core of the BEMS is a mixed integer quadratic programming (MIQP) problem solved in a rolling horizon scheme. This means that the optimization is repeated with a predetermined sample time. At each step, the operation of the HVAC system is planned for the next hours, where N_H is the number of time steps to reach the optimization horizon. The planning consists in determining the circulation pump on the water loop of the fancoils and the state of the heat pump, which consists of an on/off signal and a frequency signal communicated to the inverter-driven compressor. The optimization problem consists in the minimization of the economic objective function:

$$\min_{\Xi}\sum_{t=1}^{N_H}\left(\lambda_t^{buy}w_t^{buy} - \lambda_t^{sell}w_t^{sell}\right) + \gamma\sum_{t=1}^{N_H}\left(\delta_t\uparrow + \delta_t\downarrow\right) + \gamma_u\sum_{t=1}^{N_u}\left[\left(\Phi_t^{hc} - \Phi_t^{hc,0}\right)^2 + \left(\Phi_t^{hp} - \Phi_t^{hp,0}\right)^2\right] \tag{13}$$

subject to the constraints in Eqn 1, 2 and 3 and to those listed in the following:

$$w_t^{buy} + w_t^{pv} = w_t^{sell} + w_t^{hp} + w_t^{od} \tag{14}$$

$$\theta_t^{i,min} - \delta_t\downarrow \le \theta_t^i \tag{15}$$

$$\theta_t^i \le \theta_t^{i,max} + \delta_t\uparrow \tag{16}$$

$$\Phi_t^{hp} - \Phi_t^{hc} - UA\left(\theta_t^{hs} - \theta_t^i\right) = \frac{\rho V_{hs}c_p}{\tau}\left(\theta_t^{hs} - \theta_{t-\tau}^{hs}\right) \tag{17}$$

$$\theta_H^{hs} \ge \theta_0^{hs} \tag{18}$$

$$\Phi_t^{hp} = r_{min} Q_t^{hp,max} u_t^{hp} + Q_t^{hp,mod} \tag{19}$$

$$Q_t^{hp,mod} \leq u_t^{hp}(1 - r_{min}) Q_t^{hp,max} \tag{20}$$

$$\Phi_t^{hp} = COP_t w_t^{hp} \tag{21}$$

$$x_t^{su} \geq u_t^{hp} - u_{t-\tau}^{hp} \tag{22}$$

$$x_t^{su} \leq u_t^{hp} \tag{23}$$

$$\Phi_t^{hp} \geq x_t^{su} r_{min,su} Q_t^{hp,max} \tag{24}$$

$$Q_t^{hc} = k_{hc,0} + k_{hc,1}\theta_t^{hs} + k_{hc,2}\theta_t^{i} \tag{25}$$

$$Q_t^{hc} - \Phi_t^{hc} \leq \left(1 - u_t^{hc}\right) M \tag{26}$$

$$\Phi_t^{hc} \leq Q_t^{hc} \tag{27}$$

$$\Phi_t^{hc} \leq u_t^{hc} M \tag{28}$$

where λ_t^{buy} and λ_t^{sell} are the purchase and sale price of electricity; w_t^{buy} and w_t^{sell} represent the amount of electricity purchased and sold to the grid, and the second sum is a penalty that aims at limiting the events in which the air temperature goes beyond the boundaries of thermal comfort. The third term of the objective function was added to improve stability, i.e. to limit deviations between the optimal power profiles obtained by consecutive optimizations. This term does not sum up all the power values over the whole optimization horizon, but only the first N_u steps. In our case, deviations were penalized in the first 6 h so that N_u was set to 24. The weight γ_u was high enough to penalize significant deviations from the previous decisions, but low enough to give priority to the first two terms of the objective function. The temperature difference between the indoor air temperature and the upper/lower thermal comfort bound is defined by variables $\delta_t\uparrow$ and $\delta_t\downarrow$, respectively. Further details about the optimization can be found in an early version of this work [5]. Eq. (14) represents the electrical energy balance at building level; Eq. (15) and (16) define the boundaries of indoor thermal comfort based on the temperature setpoints fixed by the user; Eq. (17) is the thermal energy balance of the hot water tank and Eq. (18) imposes that the temperature of the water in the tank at the end of the horizon must be at least equal to its initial temperature. This choice was made to avoid continuous discharging to pursue cost minimization. Eq. (19)–(21) describe the heat pump performance; Eq. (22)–(24) set the minimum power during the heat pump start-up; Eq. (25)–(27) constrain the heat flow rate exchanged by the heat emitters to the water temperature in the tank and to the indoor air temperature, while Eq. (28) links that heat flow rate to their on–off status. The whole set of constraints includes 8 equations and 12 inequalities that must be repeated for each step t in the horizon, i.e. $\forall\, t \in [1, N_H]$. There are 16 unknown variables at each step: u_t^{hc}, u_t^{hp}, Φ_t^{hc}, Φ_t^{hp}, θ_t^{hs}, θ_t^{i}, θ_t^{s}, θ_t^{m}, w_t^{hp}, w_t^{s}, w_t^{b}, x_t^{su}, $Q_t^{hp,mod}$, $Q_t^{hc,mod}$, $\delta_t\downarrow$ and $\delta_t\uparrow$. Considering a receding horizon of 24 h with a sampling time of 15 min leads to an optimization problem $N_H = 96$ timesteps, with 8•96 = 768 equalities, 12•96 = 1152 inequalities and 16•96 = 1536 unknown variables. Therefore, the problem has (16–8)•96 = 768 degrees of freedom. The problem was formulated in Python using Gurobi solver [36] using *gurobipy* library. Appendix B provides the description of the main equality constraints (i.e. the building model) using state-space representation.

4.4. Comparison with rule-based control

The performance of the proposed MPC system was compared to that of a conventional thermostat controller. To this end, six performance indicators were used, three for the assessment of building self-sufficiency and final costs for the user, and another three for the thermal discomfort. The same indicators are calculated both for the periods with MPC and with rule-based control. In order to simplify the definition of the mentioned KPIs, it is useful to first define the heat pump self-consumption as the minimum (evaluated at each time-step) between the PV production and the HP consumption:

$$w_t^{hp,self} = \min\left(w_t^{hp}, w_t^{pv}\right) \tag{29}$$

The HP self-consumption is then used to define the economic indicators. The electrical self-consumption is then normalized either with respect to the electrical demand as in Eq. (30) or with respect to the local generation as in Eq. (31) over the whole test period considered:

$$W_{hp}^{hp,self} = \frac{\sum_t w_t^{hp,self}}{\sum_t w_t^{hp}} \tag{30}$$

$$W_{pv}^{hp,self} = \frac{\sum_t w_t^{hp,self}}{\sum_t w_t^{pv}} \tag{31}$$

A high self-consumption leads to a lower final energy cost for the user, defined as follows:

$$c^{el} = \frac{\sum_t \lambda_t^{buy} w_t^{buy}}{\sum_t w_t^{hp}} = \frac{\sum_t \lambda_t^{buy}\left(w_t^{hp} - w_t^{hp,self}\right)}{\sum_t w_t^{hp}} \tag{32}$$

Notice that the cost of energy for the user calculated with Eq. (32) does not depend on the electricity generated by the rooftop PV system. This choice was intentional, because solar radiation (and in turn PV production) varied significantly in the test periods considered. Finally,

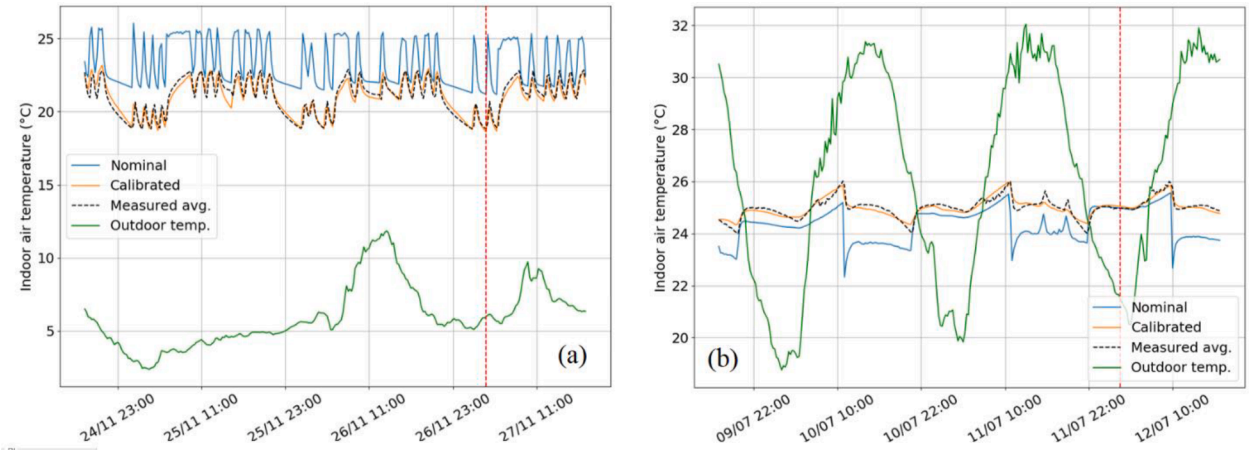

Fig. 5. Examples of model calibration: (a) in the winter season; (b) in the summer season.

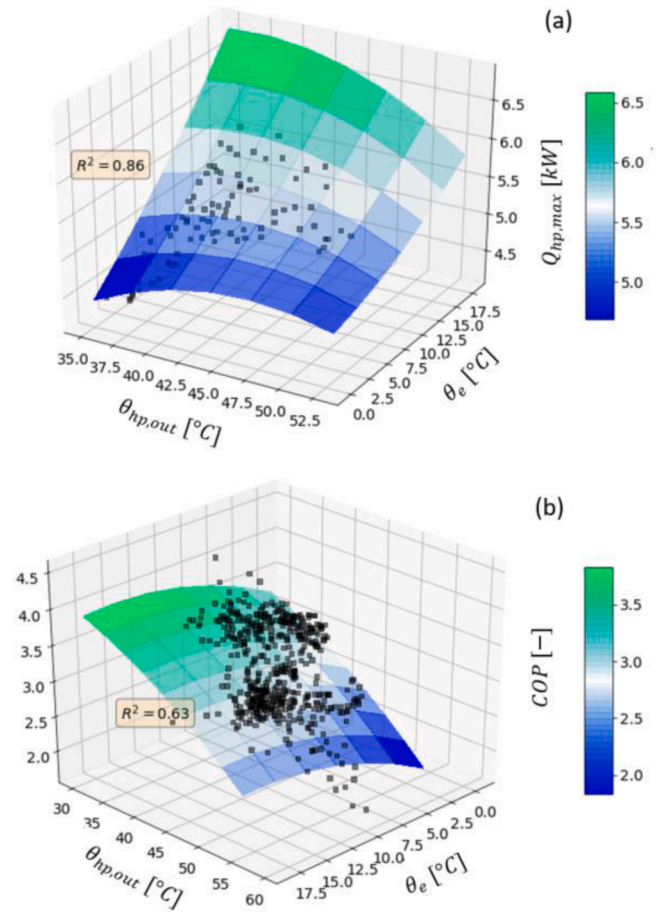

Fig. 6. a) Capacity and (b) COP of the heat pump: measurements vs linear regression model.

three indicators highlight the cost for the use in terms of thermal discomfort during the test periods considered. Thermal discomfort is generated when the indoor temperature violates the upper or lower comfort bounds, as reported in Eq. (33) and (34), respectively. The total thermal discomfort indicates the sum of both comfort violations –as in Eq. (35).

$$TD_d\uparrow = \frac{\sum_t \delta_t\uparrow}{N_d} \tag{33}$$

$$TD_d\downarrow = \frac{\sum_t \delta_t\downarrow}{N_d} \tag{34}$$

$$TD_d = TD_d\uparrow + TD_d\downarrow \tag{35}$$

Where N_d is the number of days of the considered experiment. These discomfort indexes were calculated based on the average temperature and not based on local indoor air temperatures in the four rooms.

5. Results

The results are divided into two parts: offline results analyzing the calibration and optimization outputs, and online results when the HVAC system is actually controlled by the MPC. The first part is useful to understand the behavior during real time operation. While the first part includes both heating and cooling, the second part includes the heating only.

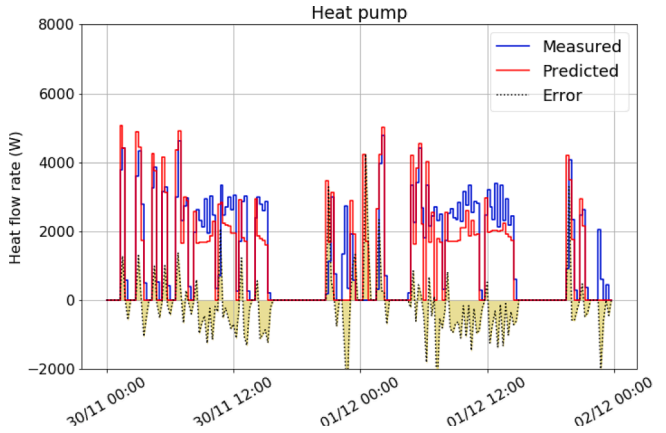

Fig. 7. Difference between heat output estimated by the simplified heat pump model and measured values.

5.1. Calibration and optimization results

The calibration results refer to both the lumped capacitance building model and the HVAC system models. The latter include the steady-state models of the air source heat pump and the fancoils and the one-node thermal storage.

5.1.1. Accuracy of the building model

Fig. 5 shows two examples of building model calibration, one for the heating season and one for the cooling season. The graphs show three indoor air temperature profiles: the blue profile has been calculated using the nominal parameters, i.e. using the information on the physical and geometrical properties of the building; the orange profile has been obtained through parameter calibration and the dashed black line is the profile of the average temperature measured in the four rooms of the Lab. The period considered in Fig. 5(a) consists of three days, from 24 to 27 November 2021. Due to the night setpoint attenuation, the period includes both oscillations within the comfort band and periods in which, due to a shift from a low setpoint (20 °C) to a high one (22 °C) in the morning (and vice versa in the evening), the frequency of the temperature signal is lower. Eighty percent of the dataset was used for training and the remaining 20% for testing, as evidenced by the dashed red vertical line. High R^2 values in both the training (84%) and testing (79%) periods highlight the ability of the calibrated model to accurately describe the transient behaviour at both frequencies. The average distance between the two profiles is quantified by RMSE, which is 0.46 K in the training period and 0.44 K in the testing period. It is interesting to note that this result is achieved despite the daily trend of the external temperature in the training period differs from that in the testing period. Fig. 5(b) shows the outcome of a calibration test similar to the previous one in duration, but carried out during the summer season, from 9 to 12 July 2021. In this case, RMSE is 0.16 K and 0.12 K in testing, while R^2 values are 79% and 82%, respectively.

5.1.2. Accuracy of HVAC system models

In order to find the coefficients of the polynomial functions, a linear regression has been implemented selecting only data corresponding to inverter frequencies greater than 59.5 Hz (the maximum frequency being 60 Hz). The square points in Fig. 6 represent the thermal power and the COP as a function of external air temperature and of the average thermal storage temperature. The coloured area in the graphs represents the second-order polynomial curve obtained by the regression to approximate the data cloud. As Fig. 6 shows, the correlation coefficient

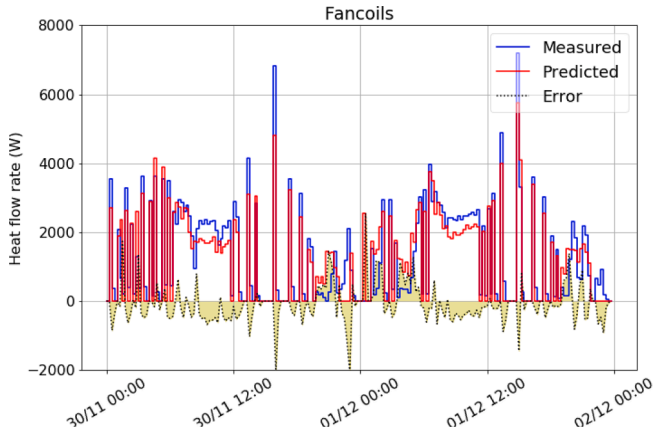

Fig. 8. Difference between heat output estimated by the simplified model of the plant and the measured values.

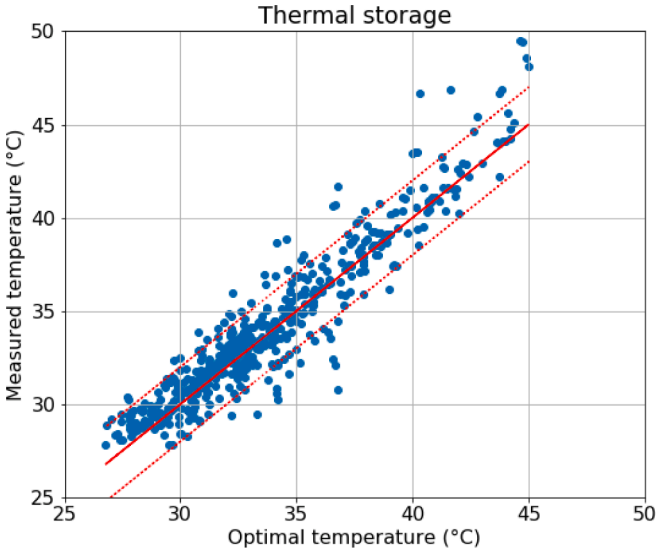

Fig. 9. Difference between water temperature in thermal storage tank estimated by simplified models and average measured values.

R^2 is 86% for the heat pump capacity and 63% for the COP in the selected period. The lower correlation index can be explained by the fact that the COP considers two phenomena with different dynamics: while the electrical power absorbed by the compressor has an almost instantaneous response considering a sampling time of one minute, the thermal power approaches its steady-state value more slowly. These transients occur mainly during compressor start-up periods. In these moments, COPs are typically lower than during steady-state operation.

Fig. 7 shows that the predicted heat flow rate supplied by the heat pump condenser (red line) is greater than the actual one (blue line) especially during periods when the heat pump is turned on and off frequently, while during periods of continuous operation the opposite occurs. For instance, during the morning and afternoon of December, 1st there is a clear underestimation of the condenser heat flow rate. This probably happens because the regression model tends to compensate the overestimation made during transients.

Fig. 8 shows the thermal power transferred from the tank to the environment through the fancoils in the same timeframe. The overestimation of the heat pump thermal power output to the heat storage tank during intermittent operation leads to overestimate the average temperature of the heat carrier fluid. As a result, one would expect the fancoils model to behave similarly to the heat pump model. Instead, during the start-ups of the fancoils there is no clear overestimation by

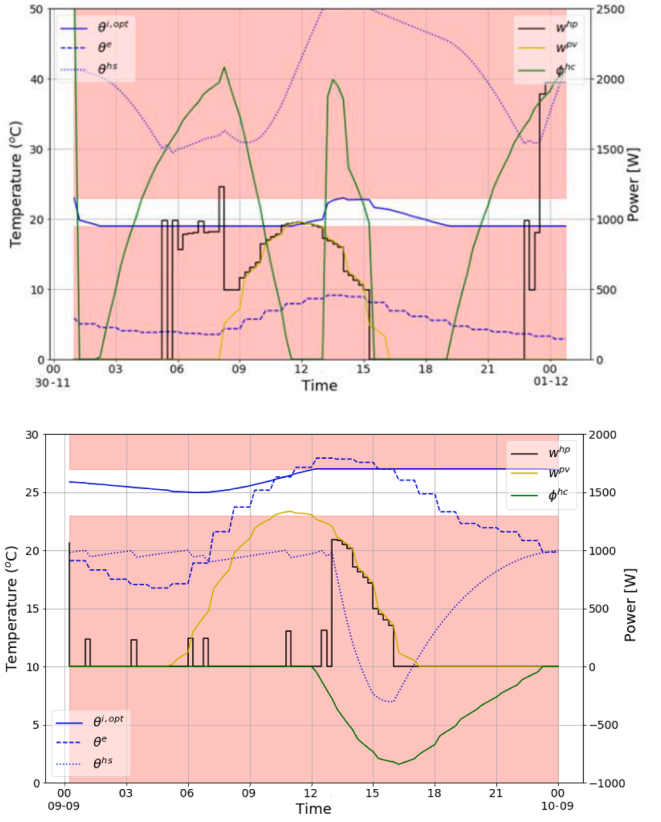

Fig. 10. Optimization results during a winter day (top) and a summer day (bottom).

the model.

This effect could be related to the stratification of the water in the storage tank. In fact, the heat carrier flows from the upper part of the tank to the heat emitters. Therefore, the temperature of the heat transfer fluid entering the fancoils is higher than the average temperature assumed in the simplified one-node model, which does not take into account the stratification. As a result, the heat transferred to the building over the period considered is greater than that predicted by the model (+13.3%), and this error is significantly lower when looking at the heat pump (+7.7%). Since both models tend to underestimate thermal output, there is not a substantial difference between the average temperature in the tank predicted by the model and the measured temperature (average of two sensors placed at different heights). Indeed, Fig. 9 shows that the error is, in most cases, between +/-2°C.

5.1.3. Optimal planning of the HVAC system

Fig. 10(a) shows the result of the optimisation performed in the laboratory at 1 am on 30/11/20 with a 24-hour horizon. The wide comfort range considered (21 ± 2 °C) was set to better appreciate the energy flexibility offered by the building structures and by the HVAC system. After an initial transient that brings the indoor air temperature (continuous blue line) from the initial state (approx. 23 °C) to the minimum of the comfort band (19 °C), the temperature remains at the minimum level throughout the day except when it is possible to self-produce energy with the PV system. In fact, when the simulated photovoltaic panels produce electricity (yellow line), the heat pump produces heat and charges the tank. The possibility of modulating the thermal output of the heat pump adapts its electrical consumption (black line) to the forecasted production of the PV modules.

The heat produced during these hours (from about 8 am to 3 pm) is not discharged directly into the room, but charges the thermal storage tank. The latter releases heat to the room both during the night and early

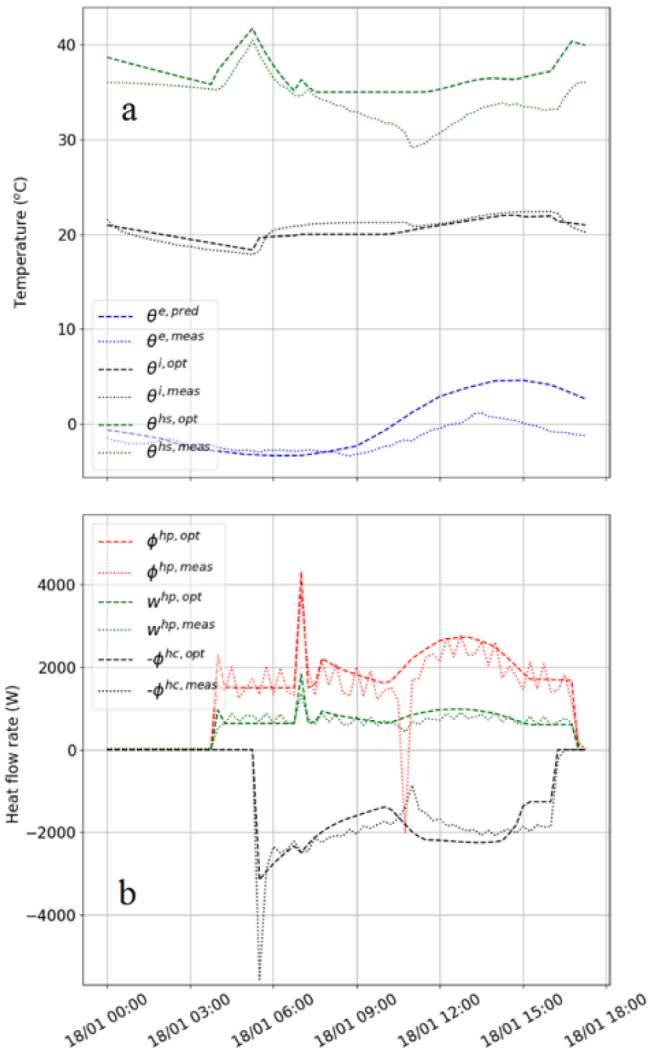

Fig. 11. Optimal planning vs measured behaviour: (a) temperatures and (b) heat flow rates.

morning hours due to the low outdoor temperature (blue dotted line), and from 1 pm onwards, when the tank has reached the maximum limit temperature and must therefore be discharged. This strategy can be appreciated by observing the green line, which represents the power profile transferred to the environment by the fan coils. This solution found by the optimiser takes maximum advantage of the combined inertia offered by the building structures and by the HVAC system. The state of charge of the tank, i.e. its average temperature θ_t^{hs} (blue dotted line) oscillates between a minimum and a maximum. In the summer season (Fig. 10(b)), the situation is mirrored: the internal temperature predicted by the optimiser is equal to the maximum allowed, except when the thermal storage can supply cold water that was produced at low cost by means of the photovoltaic system. During the night and in the morning, the external air temperature is lower than the internal one. Therefore, the heat pump only shows limited start-ups to maintain the water temperature in the tank below the maximum value allowed (20 °C). During the first afternoon hours, the heat pump exploits the electrical energy produced locally by the PV system to cool down the tank. The fancoil operation is scheduled from 12 am to 11 pm with a maximum cooling load occurring around 4 pm.

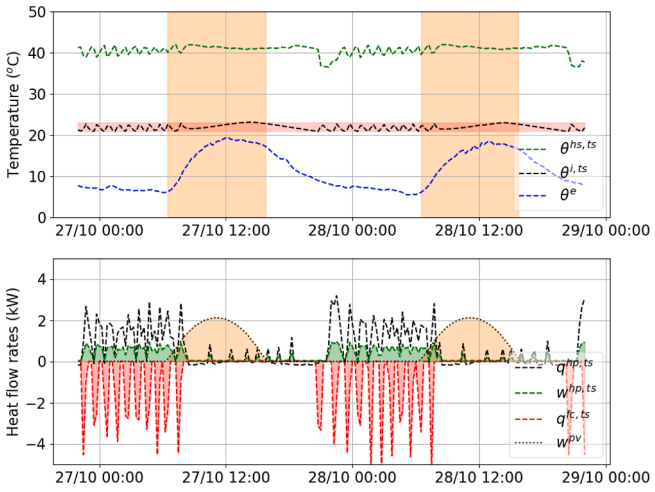

Fig. 12. Temperature and power profiles in the laboratory on 27–28/10/2021 under thermostat control.

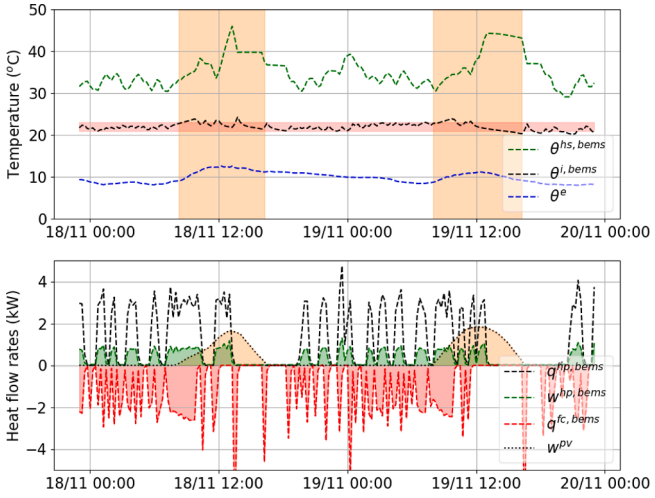

Fig. 13. Temperature and power profiles in the laboratory on 18–19/11/2021 under MPC.

5.2. Optimal control results

5.2.1. Open-loop performance

The monitored values of temperature and energy in the lab do not exactly match those predicted by the optimal planning. The difference is mainly due to the simplifications assumed in the energy balance equations describing the thermal behaviour of the system and by the inaccuracy of weather forecasts. Fig. 11 shows, by way of example, the planned and realised behaviour during a test carried out on January 18th, 2021, where dashed lines represent the predicted optimal behaviour and dotted lines stand for the actual behaviour measured in the lab. The blue lines in Fig. 11(a) show the predicted and measured outdoor air temperature. During the first hours, the measured temperature corresponds to the forecasted one, but from approximately 8 am it deviates with consequent underestimation of the heat losses due transmission and ventilation. The profiles of forecasted and actual water temperature in the tank show a diverging trend in the late morning. This can be explained by observing the heat exchange rate at the heat pump

Table 2
Summary of the MPC tests against a benchmark thermostat controller.

Indicator	Constant setpoint		Night setback	
	MPC	Thermostat	MPC	Thermostat
Period	**18–19/11**	**27–28/10**	**30/11–2/12**	**27–29/11**
$\overline{\theta}_e$(°C)	9.8	11.3	5.2	6.1
$\overline{\theta}_i$(°C)	21.9	21.9	21.1	21.0
Φ^{hc}(kWh/day)	9.03	5.17	10.50	8.82
Φ^{hp}(kWh/day)	9.37	5.11	10.71	9.05
W^{hp}(kWh/day)	2.64	2.28	3.38	3.01
COP (-)	3.55	2.24	3.17	3.01
W^{pv}(kWh/day)	2.90	4.39	2.29	1.84
$W^{hp,self}$(kWh/day)	0.83	0.34	1.20	0.58
$W_{pv}^{hp,self}$(%)	28.6%	8.9%	52.5%	31.3%
$W_{hp}^{hp,self}$(%)	31.4%	17.2%	35.5%	19.1%
c^{el}(€/kWh)	0.137	0.166	0.129	0.162
$TD_d\uparrow$(hr °C/day)	1.09	0.05	1.19	0.34
$TD_d\downarrow$(hr °C/day)	1.08	0.29	1.91	0.57
TD_d(hr °C/day)	2.17	0.34	3.10	0.91

condenser –red lines in Fig. 11(b). Despite an overall similar trend on a daily basis, the spike occurring around 10 am reaches negative values, which means that the tank switches its role from heat sink to heat source in order to perform a defrosting cycle. As a result, the water temperature in the tank drops compared to the predicted optimal trend shown by the dashed green line in Fig. 11(a). As far as the secondary side of the HVAC system is concerned, the measured and optimal heat flow rate supplied by the fancoils (Φ^{hc}) also show a similar trend on a daily basis. However, the peak due to the start-up transient is underestimated by the linear model. The electrical demand of the heat pump –green lines in Fig. 11 (b)- and the average indoor air temperature -black lines in Fig. 11(a)-, which are the most important variables for the optimization pursued by the BEMS, show a good match with the optimal values, which confirms the robustness of the proposed model predictive controller.

5.2.2. *Closed-loop performance*

The close loop performance was tested by comparing periods in which the system was operated either with the classic thermostat or with the MPC-based BEMS. The first test was run in thermostat mode during the last week of October 2021. The benchmark test with thermostat control was conducted in the third week of November, and days with the most similar weather conditions to the late October test were then chosen. In both periods the temperature setpoint inside the Lab was kept constant (23 ± 1 °C). The temperature and power profiles in both periods are shown in Fig. 12 and Fig. 13 for thermostat control and MPC, respectively. The average outdoor air temperature of the second test was 1.5 °C lower than that of late October, and the global solar radiation (measured in the horizontal plane) was almost five times lower: 0.62 kWh/m^2/day in November versus 2.90 kWh/m^2/day in late October. As a consequence, the heat demand of the laboratory at the same average indoor temperature was 57% higher in the MPC test than in the thermostat test, while the simulated photovoltaic production in the two days of October was 52% higher than in the two days of November. In addition, during the thermostat test period, the intra-day temperature fluctuation is much greater, with maximum temperatures approaching 20 °C during the day as shown in Fig. 12. The higher heat demand recorded in November was partially offset by the higher COP in the same period, in which the average temperature in the tank was 35.2 °C, against an average of 40.8 °C obtained in October by imposing setpoints 42 ± 3 °C, thus reducing the difference in electrical energy needs between the tests. Table 2 shows that, despite the little difference in the electrical energy absorbed by the heat pump in the two cases, the share of self-consumed energy is almost doubled thanks to the predictive logic, which allows to go from 17.1% to 31.4%, even with a much lower photovoltaic production and therefore in unfavorable conditions. As far

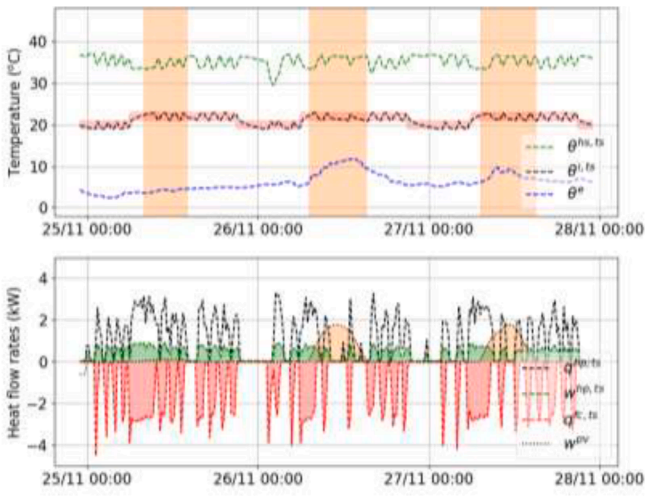

Fig. 14. Temperature and power profiles in the laboratory on 25–27/11/2021 under thermostat control.

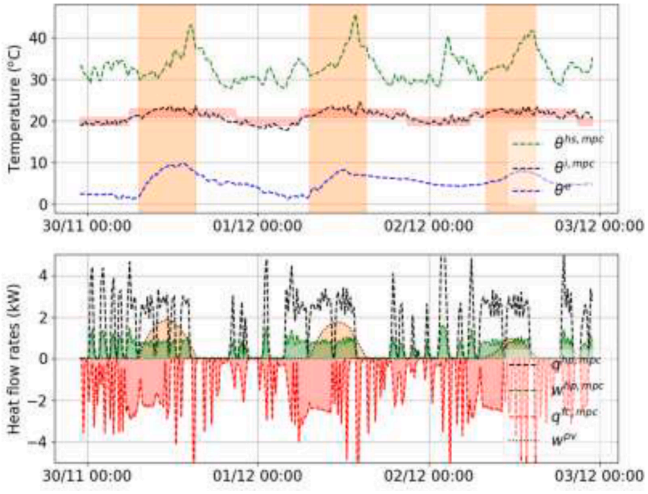

Fig. 15. Temperature and power profiles in the laboratory on 30/11–2/12/2021 under MPC.

as thermal comfort is concerned, the system shows margins for improvement as in both days there is a slight overheating in the late morning and that in the second day the average temperature falls below the lower comfort bound, although such discomfort occurs for less than one hour and not continuously. This problem can be related to the overlapping of several factors: the type of building and system, the control strategy chosen by the optimizer and the simplifications introduced by the building and system models already discussed in Sections 5.2.1 and 5.1.2. This issue also implies that the optimal decisions taken by the controller are not fully respected, as one can clearly see by comparing the indoor temperature profiles of Figs. 10 and 13. In fact, the indoor temperature during MPC operation fails to follow the lower comfort bound during periods with no PV production, which in turn increases the heat demand.

In order to test the ability of the MPC to adapt to different user preferences, the system was also tested in the case (typical in residential buildings) where the temperature setpoint is lowered during the night hours. Raising the setpoint during daylight hours means shifting consumption towards the hours of highest electricity production. This test therefore challenges the ability of the MPC to improve self-consumption compared to the traditional control system. The periods considered are three days for each control system: November 25–27, 2021 for

Table A1
Thermal characteristics of opaque building components.

Building component	Layer	Thickness [m]	Thermal Conductivity [W/(m K)]	Density [kg/m^3]	Specific heat [kJ/(kg K)]
External wall	Polyurethane	0.10	0.021	120	1.00
(U = 0.277 W/(m^2 K))	Plasterboard	0.025	0.19	660	1.00
	PVC floor	0.005	0.21	1300	1.45
Ground floor	Screed	0.05	1.4	2200	1.05
(U = 0.393 W/(m^2 K))	XPS insulation	0.05	0.037	40	1.45
	Polyethylene sheet	0.001	0.4	90	1.00
	Light concrete	0.07	0.1	520	1.05
	Concrete base	0.15	2.3	2000	1.00
Roof	Polyurethane	0.10	0.021	120	1.00
(U = 0.288 W/(m^2 K))					
False ceiling	Mineral fiber panels	0.10	0.03	120	1.00
Internal partitions	Polyurethane	0.10	0.021	120	1.00

predictive control (see Fig. 14) and November 29-December 2, 2021 for thermostat control (see Fig. 15).

Table 2 shows that self-consumption also increases significantly in this case, from 31% to 52% of the energy produced by the PV system, and from 19% to 35% of the electricity consumed. Also in this case, the cost of electricity used is significantly lowered: from 0.162 €/kWh to 0.129 €/kWh (-20%). It can be seen that the thermal energy used to heat the lab is higher in the MPC case. This is due in part to the lower average temperature over the period considered and the suboptimal control of the internal temperature due to the simplifications made to the plant models, as extensively discussed in Section 5.1.2. These deviations of the actual operation from that programmed by the optimizer also leads to exceeding the comfort limits at certain times of the day. This increase in discomfort, although low in absolute terms, is one of the most critical points found and must be improved both to ensure greater comfort to occupants, and at the same time minimize consumption. From the point of view of efficiency, however, it should be noted that the MPC is also able in this test to substantially improve the COP of the heat pump, bringing it from 3.01 to 3.38 (+12%). This improvement was obtained mainly by having a lower average temperature in the thermal buffer tank (about 2 °C less) and to an efficient compressor modulation driven by the MPC.

6. Discussion on limitations and future directions

A sensitivity analysis on the accuracy of the building model was not reported here for sake of brevity. However, it is worth reporting that several calibration runs have demonstrated that second and third-order models outperform models with one state, and that its accuracy is affected by the length of the training period and by the season considered. On average, RMSE values lower than 0.6 K have been achieved in both heating and cooling season. The type of building structure, and in particular the weight and the thermal insulation of the external walls and the share of glazed area are expected to significantly affect the accuracy of the model, as discussed in other papers [12,37]. As highlighted in Section 5.1.2, the simplified models of the HVAC system (heat pump, thermal storage and fan coils) lead to a significant discrepancy between the measured heat supplied to building and the optimal heat load profile planned by the MPC. A possible quick solution to mitigate the underestimation made by the models is to consider, during the calibration, only the periods of continuous operation, i.e. only those periods in which the heat pump is on for e.g. at least 30 minutes. An alternative solution would be to use a quasi-dynamic model considering two correlations: one for the transient regime and one for the continuous regime. A dynamic model could also be a viable option, especially if the MPC is used to provide flexibility services to the distribution or transmission grid, as shown in previous papers [38,39].

Section 5.2.2 clearly shows that the combination of such oversimplified models leads to unnecessary heat supply, which in turn implies higher thermal discomfort compared to the rule-based control. In light of these findings, further development is needed to improve the accuracy of HVAC system components and choosing an appropriate number of training days for building calibration so that both controllable inputs and disturbances in the learning phase are similar to those in the testing phase.

These sections have the merit of discussing in depth the consequences of oversimplified models based on monitored results, but their limitation is that they have not quantified the relative contribution of each model to the overall deviations reported in the results. Indeed, thermal discomfort violations could be related not only to the underestimation of the heat supplied to the indoor space but also to the inaccuracy of the building model. The latter is the focus of an analysis that will be presented in a separate work.

Moreover, the application of the MPC approach proposed in this paper is limited to single thermal zones, and should be adjusted in those buildings where multiple thermal zones must be controlled separately.

It is also important to consider the effect of uncertainty in the forecast data, especially concerning solar radiation due to its effect on PV production and in turn on the objective function of economic MPC. This aspect could not be analysed here because the PV system has been installed months after the experiments. In the future, the comparison between predicted PV production using solar radiation forecasts and the actual PV production will make it possible to close this gap. Another important source of uncertainty in the disturbances would be introduced by active users, who were not considered in the research work presented in this article. Such additional disturbance is particularly relevant in new and refurbished buildings, where internal heat gains and windows opening patterns affect the heating load profile significantly.

7. Conclusions

The research activity has shown that it is possible to manage the electrical loads of a lightweight all-electric building with a predictive logic to maximize the use of renewable energy produced on site through the photovoltaic system, while obtaining significant savings for the end user. To this end, the thermal inertia of the building-plant system has been exploited to shift the electrical loads for space heating with different comfort constraints.

The results showed that during the winter season it is possible to increase the self-consumption from 17-19% to 31–35% depending on the climatic conditions and the comfort conditions required by the user. This strategy allows to obtain savings on electricity in a range of 10–17% compared to a conventional control.

This result is significant since the analysed building is not equipped with a battery for electrical energy storage, and is a lightweight building characterized by low thermal inertia. Therefore, the same controller is expected to obtain more significant savings in heavyweight buildings with a different heat emission system (radiators or radiant systems).

On the other hand, the study highlighted some inaccuracies when using steady-state models for a fast-responsive HVAC systems with

intermittent behaviour. An analysis of the results showed that, due to the regression performed considering data during both transient and continuous operation, the models significantly underestimated the actual heat output of both the heat pump and the fan coils. Such inaccuracies contributed to 3–6 times higher comfort violations and a higher amount of thermal energy supplied for space heating, thus decreasing the overall performance of the MPC. The increase in energy consumption was also caused by colder weather recorded during MPC tests (lower outdoor temperature and in one case lower solar radiation).

The next steps will include the formulation of improved HVAC models, as well as the inclusion of DHW production and ventilation among the controlled variables. Experiments will be repeated both in the heating and cooling season. Finally, it would be important to test the control system inside a real building inhabited by people to investigate how user behaviour and forecasts' uncertainty affect the results obtained so far.

Declaration of Competing Interest

The authors declare that they have no known competing financial interests or personal relationships that could have appeared to influence the work reported in this paper.

Acknowledgements

This work has been financed by the Research Fund for the Italian Electrical System under the program agreement between Ricerca Sistema Energetico S.p.A. and the Ministry of Economic Development. The Authors would like to thank Nicolò Mazzi for his contribution in the preliminary phase of this work, and Massimo Fiorentini for the insightful comments given in the revision phase.

Appendix A. Thermal properties of building components

The stratigraphy of the opaque building components and their thermal transmittance are summarized in Table A.1. The declared thermal conductivity of the polyurethane panels is 0.021 W/(m K). The thermal transmittances in the Table were calculated using a more realistic value of 0.030 W/(m K). The thermal transmittance of the door and of the windows are 1.54 and 2.29 W/(m^2 K), respectively.

Appendix B. State-space representation

The state-space representation of the building model is the following:

$$\dot{x} = Ax + Bu \tag{B.1}$$

where × and u represent the states and the inputs of the model, respectively. In this case, the states are $x^T = [\theta^i, \theta^s, \theta^m]$ and the inputs are $u^T = [\theta^{sup}, \theta^{e,eq}, \Phi^{ia}, \Phi^{st}, \Phi^m, \Phi^{hc}, \delta\uparrow, \delta\downarrow]$. Among the inputs, the first five entries are disturbances that depend on the weather conditions, i.e. external air temperature and solar radiation, and internal gains due to human activities in the building. In particular, θ^{sup} is the supply air due to infiltration/ventilation, $\theta^{e,eq}$ is the equivalent sol–air temperature defined in Eq. (4) and $\Phi^{ia}, \Phi^{st}, \Phi^m$ are a combination of solar and internal heat gains, as defined in Eqs. (8)–(10). The last component of u is the controllable input of the MPC, i.e. the heat flow rate supplied to the building through the fancoil units (Φ^{hc}). With the help of Eqs. (1)–(3), the state matrix and the input matrix B can be defined as shown in Eqs. (B.2)–(B.3).

$$A = \begin{bmatrix} -\dfrac{H_{ve} + H_{tr,is}}{C_i} & \dfrac{H_{tr,is}}{C_i} & 0 \\ \dfrac{H_{tr,is}}{C_s} & -\dfrac{H_{tr,w} + H_{tr,is} + H_{tr,ms}}{C_s} & \dfrac{H_{tr,ms}}{C_s} \\ 0 & \dfrac{H_{tr,ms}}{C_m} & -\dfrac{H_{tr,em} + H_{tr,ms}}{C_m} \end{bmatrix} \tag{B.2}$$

$$B = \begin{bmatrix} \dfrac{H_{ve}}{C_i} & 0 & \dfrac{1}{C_i} & 0 & 0 & \dfrac{f_{conv}}{C_i} \\ 0 & \dfrac{H_{tr,w}}{C_s} & 0 & \dfrac{1}{C_s} & 0 & \dfrac{1 - f_{conv}}{C_s} \\ 0 & \dfrac{H_{tr,em}}{C_m} & 0 & 0 & \dfrac{1}{C_m} & 0 \end{bmatrix} \tag{B.3}$$

The formulation above is a reduced version of the whole set of constraints (reported in Section 4.3) that only considers the dynamic building model. The whole problem should also account for additional disturbances such as the PV production w^{pv} and additional controllable inputs such as the thermal power supplied by the air source heat pump Φ^{hp}, its power consumption w^{hp} and the penalties for thermal comfort violation, $\delta\uparrow$ and $\delta\downarrow$.

References

[1] J. Barton, S. Huang, D. Infield, M. Leach, D. Ogunkunle, J. Torriti, M. Thomson, The evolution of electricity demand and the role for demand side participation, in buildings and transport, Energy Policy. 52 (2013) 85–102, https://doi.org/10.1016/j.enpol.2012.08.040.

[2] M. Pierro, R. Perez, M. Perez, D. Moser, C. Cornaro, Italian protocol for massive solar integration: Imbalance mitigation strategies, Renewable Energy 153 (2020) 725–739, https://doi.org/10.1016/j.renene.2020.01.145.

[3] A. Arteconi, D. Patteeuw, K. Bruninx, E. Delarue, W. D'haeseleer, L. Helsen, Active demand response with electric heating systems: Impact of market penetration, Appl. Energy 177 (2016) 636–648.

[4] J. Vivian, U. Chiodarelli, G. Emmi, A. Zarrella, A sensitivity analysis on the heating and cooling energy flexibility of residential buildings, Sustainable Cities and Society. 52 (2020), 101815, https://doi.org/10.1016/j.scs.2019.101815.

[5] J. Vivian, N. Mazzi, An algorithm for the optimal management of air-source heat pumps and PV systems, Journal of Physics: Conference Series. 1343 (2019) 012069. https://doi.org/10.1088/1742-6596/1343/1/012069.

[6] J. Vivian, E. Prataviera, F. Cunsolo, M. Pau, Demand Side Management of a pool of air source heat pumps for space heating and domestic hot water production in a residential district, Energy Convers. Manage. 225 (2020), 113457, https://doi.org/10.1016/j.enconman.2020.113457.

[7] Z.E. Lee, Q. Sun, Z. Ma, J. Wang, J.S. MacDonald, K. Max Zhang, Providing Grid Services With Heat Pumps: A Review, ASME Journal of Engineering for Sustainable Buildings and Cities. 1 (2020), https://doi.org/10.1115/1.4045819.

[8] M. Fiorentini, G. Serale, G. Kokogiannakis, A. Capozzoli, P. Cooper, Development and evaluation of a comfort-oriented control strategy for thermal management of mixed-mode ventilated buildings, Energy Build. 202 (2019), 109347, https://doi.org/10.1016/j.enbuild.2019.109347.
[9] T.Q. Péan, J. Salom, R. Costa-Castelló, Review of control strategies for improving the energy flexibility provided by heat pump systems in buildings, J. Process Control 74 (2019) 35–49, https://doi.org/10.1016/j.jprocont.2018.03.006.
[10] G. Serale, M. Fiorentini, A. Capozzoli, D. Bernardini, A. Bemporad, Model Predictive Control (MPC) for Enhancing Building and HVAC System Energy Efficiency: Problem Formulation, Applications and Opportunities, Energies. 11 (2018) 631, https://doi.org/10.3390/en11030631.
[11] Y. Zong, G.M. Böning, R.M. Santos, S. You, J. Hu, X. Han, Challenges of implementing economic model predictive control strategy for buildings interacting with smart energy systems, Appl. Therm. Eng. 114 (2017) 1476–1486, https://doi.org/10.1016/j.applthermaleng.2016.11.141.
[12] D.H. Blum, K. Arendt, L. Rivalin, M.A. Piette, M. Wetter, C.T. Veje, Practical factors of envelope model setup and their effects on the performance of model predictive control for building heating, ventilating, and air conditioning systems, Appl. Energy 236 (2019) 410–425, https://doi.org/10.1016/j.apenergy.2018.11.093.
[13] C. Verhelst, F. Logist, J. Van Impe, L. Helsen, Study of the optimal control problem formulation for modulating air-to-water heat pumps connected to a residential floor heating system, Energy Build. 45 (2012) 43–53, https://doi.org/10.1016/j.enbuild.2011.10.015.
[14] M. Hu, F. Xiao, J.B. Jørgensen, R. Li, Price-responsive model predictive control of floor heating systems for demand response using building thermal mass, Appl. Therm. Eng. 153 (2019) 316–329, https://doi.org/10.1016/j.applthermaleng.2019.02.107.
[15] G. Bianchini, M. Casini, A. Vicino, D. Zarrilli, Demand-response in building heating systems: A Model Predictive Control approach, Appl. Energy 168 (2016) 159–170, https://doi.org/10.1016/j.apenergy.2016.01.088.
[16] G. Bianchini, M. Casini, D. Pepe, A. Vicino, G.G. Zanvettor, An integrated model predictive control approach for optimal HVAC and energy storage operation in large-scale buildings, Appl. Energy 240 (2019) 327–340, https://doi.org/10.1016/j.apenergy.2019.01.187.
[17] J. Drgoňa, D. Picard, M. Kvasnica, L. Helsen, Approximate model predictive building control via machine learning, Appl. Energy 218 (2018) 199–216, https://doi.org/10.1016/j.apenergy.2018.02.156.
[18] S. Kuboth, F. Heberle, A. König-Haagen, D. Brüggemann, Economic model predictive control of combined thermal and electric residential building energy systems, Appl. Energy 240 (2019) 372–385, https://doi.org/10.1016/j.apenergy.2019.01.097.
[19] W. Wang, Q. Zhou, C. Pan, F. Cao, Energy-efficient operation of a complete Chiller-air handing unit system via model predictive control, Appl. Therm. Eng. 201 (2022), 117809, https://doi.org/10.1016/j.applthermaleng.2021.117809.
[20] R.A. Kishore, M.V.A. Bianchi, C. Booten, J. Vidal, R. Jackson, Modulating thermal load through lightweight residential building walls using thermal energy storage and controlled precooling strategy, Appl. Therm. Eng. 180 (2020), 115870, https://doi.org/10.1016/j.applthermaleng.2020.115870.
[21] S. Cesari, G. Emmi, M. Bottarelli, A weather forecast-based control for the improvement of PCM enhanced radiant floors, Appl. Therm. Eng. 206 (2022), 118119, https://doi.org/10.1016/j.applthermaleng.2022.118119.
[22] A. Mirakhorli, B. Dong, Model predictive control for building loads connected with a residential distribution grid, Appl. Energy 230 (2018) 627–642, https://doi.org/10.1016/j.apenergy.2018.08.051.
[23] H. Golmohamadi, K.G. Larsen, P.G. Jensen, I.R. Hasrat, Hierarchical flexibility potentials of residential buildings with responsive heat pumps: A case study of Denmark, Journal of Building Engineering. 41 (2021), 102425, https://doi.org/10.1016/j.jobe.2021.102425.
[24] J. Hou, H. Li, N. Nord, G. Huang, Model predictive control under weather forecast uncertainty for HVAC systems in university buildings, Energy Build. 257 (2022), 111793, https://doi.org/10.1016/j.enbuild.2021.111793.
[25] Z. Lee, K. Gupta, K.J. Kircher, K.M. Zhang, Mixed-integer model predictive control of variable-speed heat pumps, Energy Build. 198 (2019) 75–83, https://doi.org/10.1016/j.enbuild.2019.05.060.
[26] W. Wang, B. Hu, R. Wang, M. Luo, G. Zhang, B. Xiang, Model predictive control for the performance improvement of air source heat pump heating system via variable water temperature difference, International Journal of Refrigeration. (2022) S0140700722000548. https://doi.org/10.1016/j.ijrefrig.2022.03.001.
[27] J. Joe, P. Karava, A model predictive control strategy to optimize the performance of radiant floor heating and cooling systems in office buildings, Appl. Energy 245 (2019) 65–77, https://doi.org/10.1016/j.apenergy.2019.03.209.
[28] A. Afram, F. Janabi-Sharifi, Supervisory model predictive controller (MPC) for residential HVAC systems: Implementation and experimentation on archetype sustainable house in Toronto, Energy Build. 154 (2017) 268–282, https://doi.org/10.1016/j.enbuild.2017.08.060.
[29] F. Bünning, B. Huber, P. Heer, A. Aboudonia, J. Lygeros, Experimental demonstration of data predictive control for energy optimization and thermal comfort in buildings, Energy Build. 211 (2020), 109792, https://doi.org/10.1016/j.enbuild.2020.109792.
[30] F. Bünning, J. Warrington, P. Heer, R.S. Smith, J. Lygeros, Frequency regulation with heat pumps using robust MPC with affine policies, IFAC-PapersOnLine. 53 (2020) 13210–13215, https://doi.org/10.1016/j.ifacol.2020.12.147.
[31] M. Fiorentini, J. Wall, Z. Ma, J.H. Braslavsky, P. Cooper, Hybrid model predictive control of a residential HVAC system with on-site thermal energy generation and storage, Appl. Energy 187 (2017) 465–479, https://doi.org/10.1016/j.apenergy.2016.11.041.
[32] G. Serale, M. Fiorentini, A. Capozzoli, P. Cooper, M. Perino, Formulation of a model predictive control algorithm to enhance the performance of a latent heat solar thermal system, Energy Convers. Manage. 173 (2018) 438–449, https://doi.org/10.1016/j.enconman.2018.07.099.
[33] International Organization for Standardization, ISO 13790: Energy performance of buildings: calculation of energy use for space heating and cooling., 2008.
[34] W.F. Holmgren, C.W. Hansen, M.A. Mikofski, pvlib python: a python package for modeling solar energy systems, Journal of Open Source Software. 3 (2018) 884. https://doi.org/10.21105/joss.00884.
[35] P. Ineichen, R. Perez, A new airmass independent formulation for the Linke turbidity coefficient, Sol. Energy 73 (2002) 151–157, https://doi.org/10.1016/S0038-092X(02)00045-2.
[36] Gurobi Optimizer Reference Manual, Gurobi Optimization, LLC, 2021. https://www.gurobi.com.
[37] S. Prívara, J. Cigler, Z. Váňa, F. Oldewurtel, C. Sagerschnig, E. Žáčeková, Building modeling as a crucial part for building predictive control, Energy Build. 56 (2013) 8–22, https://doi.org/10.1016/j.enbuild.2012.10.024.
[38] E. Vrettos, G. Andersson, Scheduling and Provision of Secondary Frequency Reserves by Aggregations of Commercial Buildings, IEEE Trans. Sustain. Energy. 7 (2016) 850–864, https://doi.org/10.1109/TSTE.2015.2497407.
[39] Y.-J. Kim, L.K. Norford, J.L. Kirtley, Modeling and Analysis of a Variable Speed Heat Pump for Frequency Regulation Through Direct Load Control, IEEE Trans. Power Syst. 30 (2015) 397–408, https://doi.org/10.1109/TPWRS.2014.2319310.